Optimizing Non-Invasive Glucose Monitoring with Monte Carlo Simulations

Jared Logan

A capstone report submitted to the faculty of
Brigham Young University
in partial fulfillment of the requirements for the degree of

Bachelor of Science

Robert Davis and Richard Vanfleet, Advisors

Department of Physics and Astronomy

Brigham Young University

Copyright © 2022 Jared Logan

All Rights Reserved

ABSTRACT

Optimizing Non-Invasive Glucose Monitoring
with Monte Carlo Simulations

Jared Logan
Department of Physics and Astronomy, BYU
Bachelor of Science

Short wavelength infrared (SWIR) optical measurements may make non-invasive glucose monitoring possible. This would make glucose-tracking for individuals with diabetes easier and less painful. Our research group has developed a miniaturized SWIR spectrometer with the goal of non-invasive arterial blood glucose monitoring on the wrist. Understanding the transport of SWIR light to and from the artery is essential for the creation of this technology. Using Monte Carlo simulation techniques, we modeled how infrared light from a light source will propagate into, and out of, the wrist. Using the data collected, we found that the signal-to-shot-noise ratio is maximized for a 7mm long spectrometer when the light source and spectrometer are 4mm apart with one on each side of the radial artery.

Keywords: non-invasive, glucose monitoring, Monte Carlo, short wavelength infrared, SWIR, infrared, spectrometer, blood spectroscopy

ACKNOWLEDGMENTS

I would like to thank the Brigham Young University Physics and Astronomy department for all of the support and guidance that they have given me for this project. In particular, I would like to thank Dr. Robert Davis, Dr. Richard Vanfleet, and Evan Dodson for all of their support. They trained me and advised me through this whole process. Without their help, this capstone project would not have been possible. Finally, I'd like to thank Tula Health. They have provided financial support for this project and have been instrumental to the breakthroughs that our group has made.

Contents

Table of Contents **vii**

1 Introduction **1**
1.1 The Current State of Glucose Monitoring 1
1.2 Non-Invasive Glucose Monitoring 2

2 Methods **3**
2.1 Monte Carlo Simulations 3
2.2 The Model Geometry 4
2.3 Signal-to-Shot-Noise Calculations 6
2.4 Simulations 7

3 Results **9**

Appendices **15**
.1 Appendix 15

Bibliography **19**

Chapter 1

Introduction

1.1 The Current State of Glucose Monitoring

A problem that is particularly prevalent in today's society is diabetes. Almost everyone knows someone who is diabetic, and it is challenging for individuals affected by it. While there are already many technologies and resources available to help those with diabetes, there are still many problems that need to be resolved when it comes to glucose monitoring. Glucose monitoring is usually accomplished using two different methods. The first method is a finger stick monitor. These devices require the patient to stick their finger with a lancet to get a blood sample. The blood sample is then inserted into a glucose monitoring device, and the device measures the amount of glucose in that blood sample [1]. The second method uses a disposable CGM sensor instead of a finger stick. It is a patch with a needle on the underside that is inserted into the skin when the patch is first applied. The patch is able to take constant readings of the patient by taking interstitial fluid samples as often as needed without re-sticking the patient every time [1]. While both of these methods are sufficient for helping the patients monitor the glucose levels in their blood, there are two main problems. First, the process is uncomfortable at best, and painful at worst. For the finger stick device in particular,

every measurement requires the patient to stick their finger with a needle. The CGM patch is better, as it only requires a single stick on the body, but it is also expensive. The patches must be replaced between 3 days and 2 weeks after application, and the cost of constantly replacing them adds up quickly. In addition, the CGM patch only measures interstitial fluid, which has been shown to be less accurate for quick changes in glucose levels [1]. Our goal is to make glucose monitoring less painful and less expensive by creating a non-invasive glucose monitor to read glucose levels through the skin.

1.2 Non-Invasive Glucose Monitoring

Our non-invasive glucose sensor relies on infrared spectrometry to read the glucose levels under the skin. The non-invasive sensor outputs near-infrared light into the skin with wavelengths between 1000nm and 2000nm. A spectrometer a couple millimeters away from the light source measures the intensities of the wavelengths as they exit the skin at that point. In previous research, in vitro measurements have shown that there is a spectral change in blood caused by large changes in the glucose level of that blood [2]. Our hope is that the glucose sensor will be able to utilize this correlation, and the measurements from the detector, to determine how much glucose is in the blood under the skin. The goal is that the sensor will be used on the wrist where a typical watch would be worn. This research aims to examine where the light source and detector should be placed relative to the radial artery to maximize the signal-to-shot-noise ratio expected at the sensor's spectrometer.

Chapter 2

Methods

2.1 Monte Carlo Simulations

To determine where to put the light source and detector relative to the radial artery we used Monte Carlo simulations. A Monte Carlo simulation is a powerful computational method which can be used to estimate how light would propagate through complex media. The particular software we used is called FullMonteSW [3]. The software models light propagation through highly-scattering media, such as biological tissues, by simulating "photon packets" and their trajectories. Several examples of possible photon packet trajectories are shown in Fig. 2.1. Each packet of photons is sent into the material from a virtual light source. While the photon packet is moving through the material, it will occasionally scatter. At each scattering event, the packet changes its direction. It also has a chance to lose some energy at every step. How much energy is lost and how much the direction is changed is determined probabilistically based on the properties of the tissue. A single photon packet will follow a path similar to a random walk through the tissue, losing energy along the way. When millions or billions of photon packets are simulated, the combined paths of all of the packets give a good picture of how the light will propagate through the tissue. Using this method,

we were able to simulate light sources and detectors at a variety of positions across a virtual wrist to determine how large of a signal we would expect to see in the spectrometer.

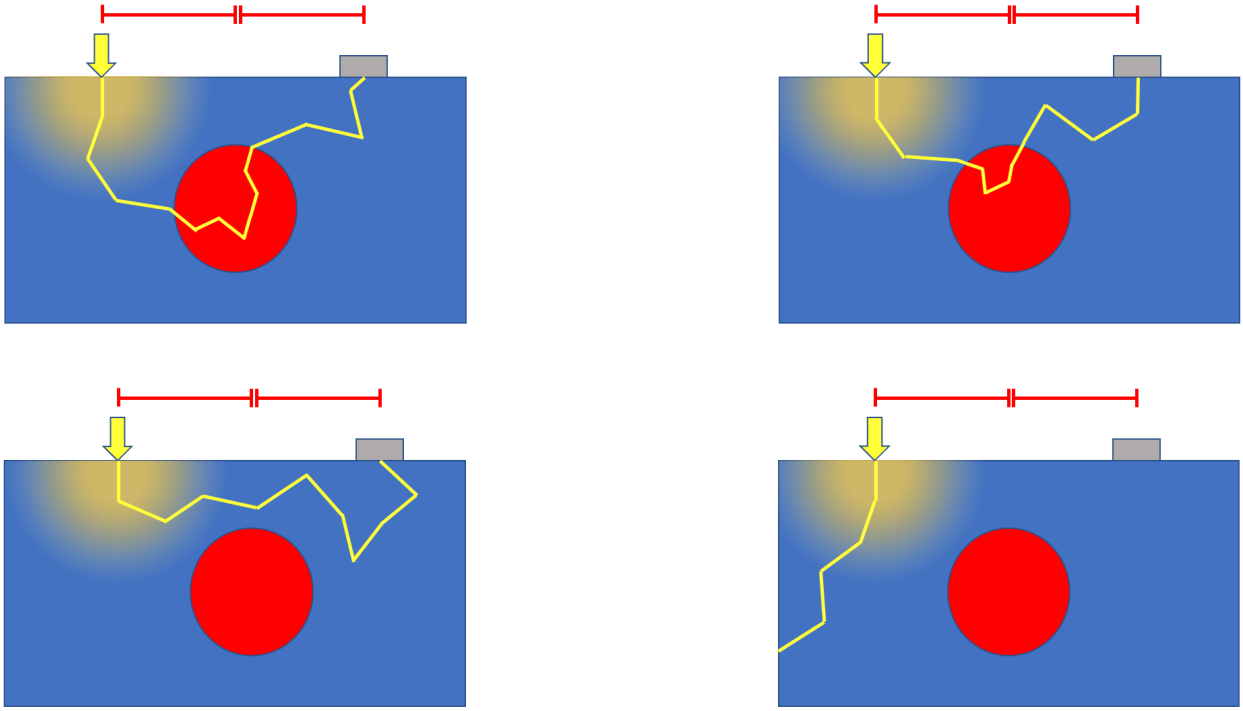


Figure 2.1 Each of these 4 images demonstrate an example path a photon packet could take through this set of highly-scattering tissue. For these example models, the blue areas represent subcutaneous adipose tissue and skin, while the red areas represent blood. The yellow arrow represents a light source on the surface of the skin. The gray rectangle represents the point on the skin where the optical detector is placed. Each path can vary drastically from the others, but their combined weights give a clear picture of what proportion of the light reaches each area of the tissue.

2.2 The Model Geometry

This section will discuss the model used, and its particular physiological parameters. The model used here is fairly simplistic in nature, though it can be made more complex if future work requires it. The geometry is shown in Fig. 2.2, and represents a section of the human wrist that is directly over the radial artery. The artery radius is able to be adjusted to model both the systolic and diastolic

artery. The particular dimensions and physiological parameters used are displayed in Table 2.1. The optical properties of the geometry we used came from the results in the paper written by Bashkatov [4].

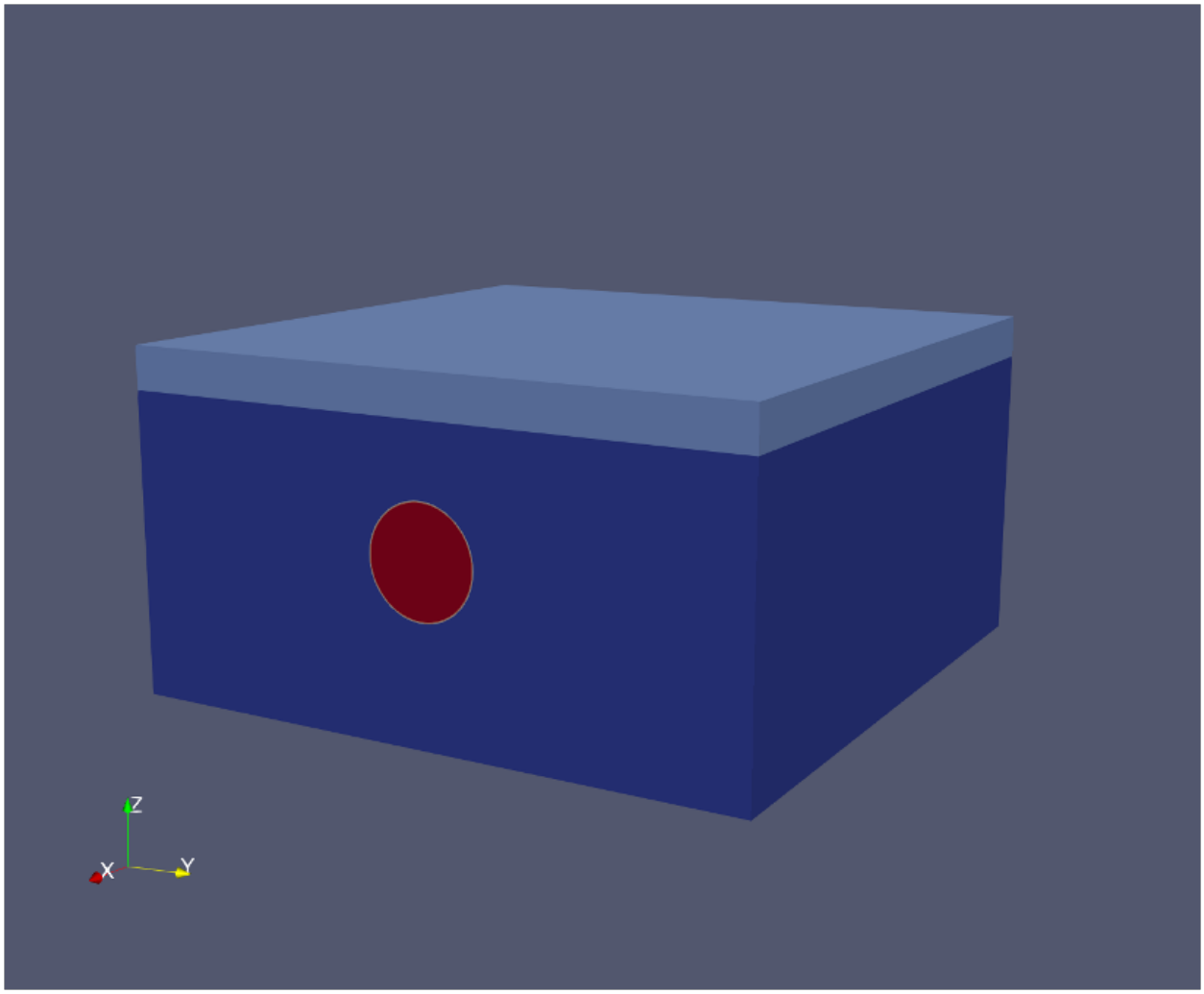


Figure 2.2 The complete model used in our simulations. The light blue area represents the skin, the dark blue area represents the subcutaneous adipose tissue surrounding the artery, and the red area represents the radial artery.

Geometry Dimensions	
Dimension	Distance
Geometry Length	15.00 mm
Geometry Width	15.00 mm
Geometry Height	8.00 mm
Skin Thickness	1.00 mm
Artery Depth (to top)	2.70 mm
Diastolic Artery Diameter	2.50 mm
Systolic Artery Diameter	2.54 mm

Table 2.1 The dimensions of the model geometry. These parameters represent the physiological dimensions of the human wrist directly over the radial artery. Since the actual values vary from person to person, the values used here are rounded for simplicity [5] [6] [7] [8] [9] [10].

2.3 Signal-to-Shot-Noise Calculations

For this work, we are interested in maximizing the signal-to-shot-noise ratio (hereafter referred to as the SNR). While there will be other noise in the sensor due to electronic limitations, the purpose of this work is to determine where the light source and detector should be placed when the device is shot-noise limited. The equation governing SNR is:

$$SNR = \frac{Signal}{ShotNoise} \tag{2.1}$$

In our case, both the signal and the shot noise are measured as a number of photons. The signal is the number of photons that reached the detector from the light source after first passing through the artery. We will refer to this light as "arterial" light. Any light that did not reach the artery does not contain information about the glucose level in the blood. For this reason, any light that reached the detector without first reaching the artery is considered "background" light. Shot noise is

proportional to the square root of the total number of photons to reach the detector. Therefore, our equation for SNR becomes:

$$SNR = \frac{Arterial}{\sqrt{Arterial + Background}} \tag{2.2}$$

2.4 Simulations

Using this geometry, we simulated a variety of wavelengths, light source positions, and detector positions. The wavelength was varied from 1000nm to 1600nm at 100nm intervals for a total of 7 different wavelengths. The light source and detectors were simulated in the positions shown in Fig. 2.3. Notice that the 5 light sources are placed along the left edge of the geometry surface 1mm apart. They are placed along the edge of the geometry because of the symmetry of these simulations. Any detectors on the left of the light sources would have had identical results to the corresponding detector mirrored on the right of the light sources. By only simulating the detectors on one side of the light sources, there is a quicker computation time for each simulation. Each light source position had to be simulated separately for each wavelength, while the 81 detector positions were able to be compiled together into one simulation. 220 million photon packets were used in each of the 35 simulations for a total of 7.7 billion photon packets. The calculations for SNR assumed that 0.1 Joules of energy was inserted into the skin for each simulation. The output was a file showing how much arterial light reached each detector, how much background light reached each detector, and the calculated SNR of each detector.

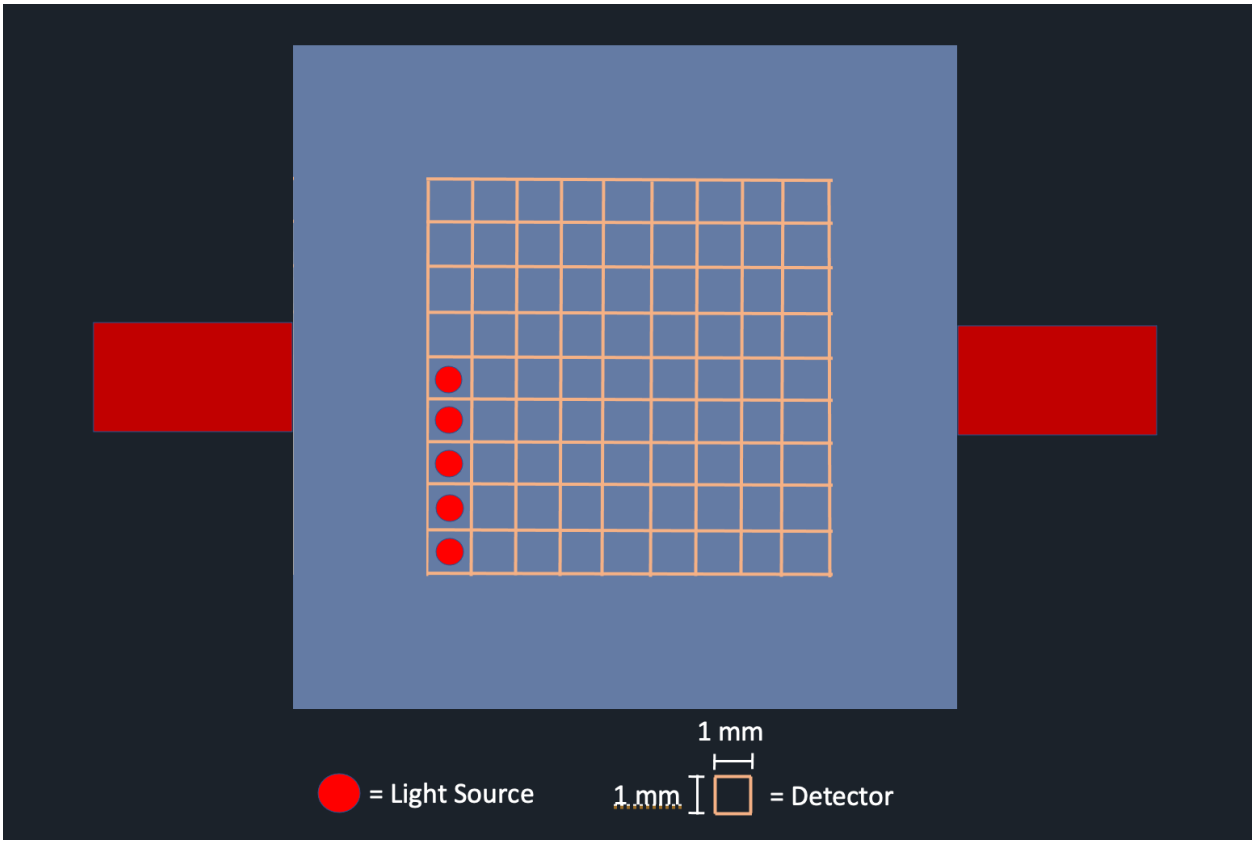


Figure 2.3 This is a top down view of the model geometry. The blue represents the skin and the red bar underneath represents the artery flowing underneath the skin. Each red dot represents one of the simulated light source positions. Each light source position is separated by 1mm. Each tan-gray square represents a detector on the surface of the skin. The detectors are each 1mm x 1mm, and together they cover a 9mm x 9mm area.

Chapter 3

Results

The results of these simulations will be shown using heatmaps for the SNR across the skin. Fig. 3.1 shows an example heatmap to demonstrate each aspect of the figure, and the complete set of simulations are contained in Appendix .1.

We will focus on just a couple of the simulations which best highlight the results of this project. To start, Fig. 3.2 below compares the SNR across wavelengths with a fixed light source position 2mm from the artery. Since the 1400nm and 1500nm simulations were both close to the water extinction coefficient, many of the detectors never received light from the light source. For this reason, SNR could not be calculated and those simulations will be omitted. The scale is the same for each heatmap, which means that a variation in color between wavelengths indicates a real change in SNR. Notice that the particular shape of the heatmap (peaks, valleys, slopes) are all in the same position regardless of wavelength. This is true for all of the different light sources. Wavelength does not seem to affect the shape of the heatmaps, only the relative values of the SNR for each of the detectors. Even 1600nm, which has a much smaller SNR than the other wavelengths, has the same shape when the scaling is zoomed in (see Appendix .1). The 1100nm simulation had the best SNR overall, while 1600nm had the lowest SNR. This pattern inversely correlates with the absorption coefficient of blood at these wavelengths, as we would expect. The more absorptive wavelengths

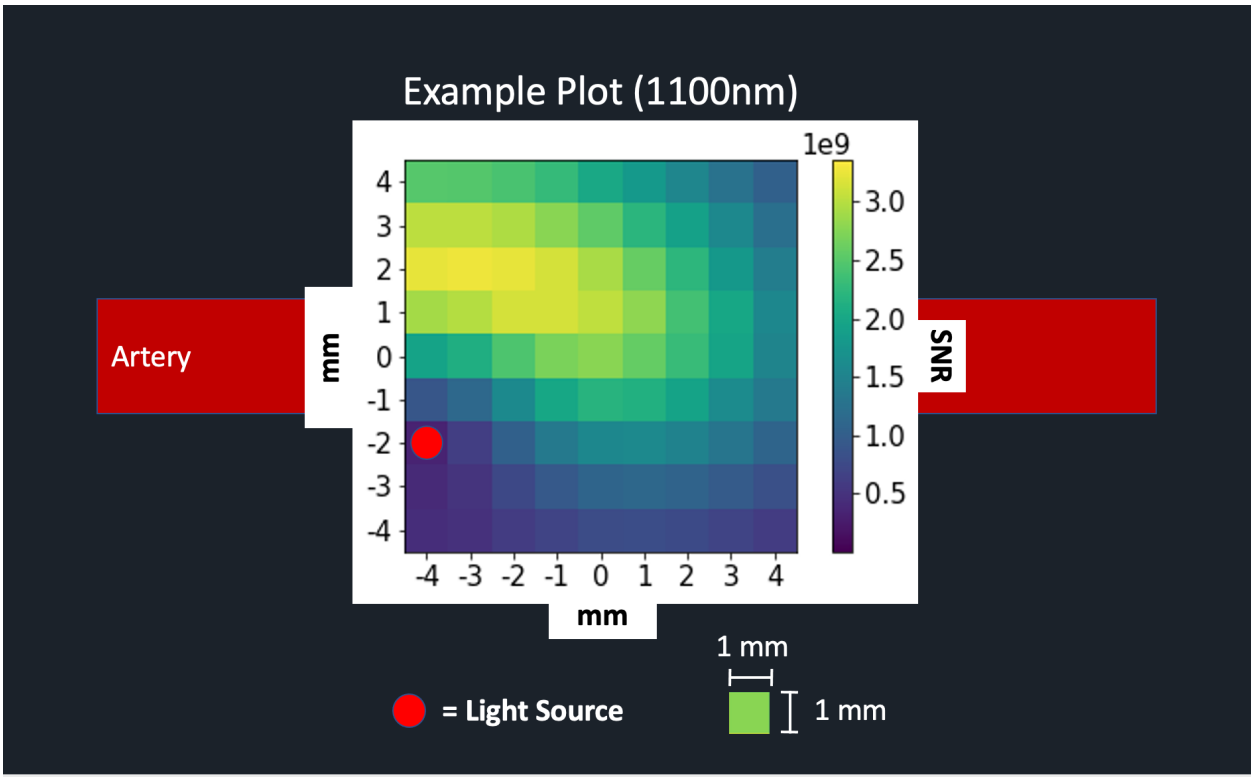


Figure 3.1 This is an example of what a simulation outputs. This particular simulation used a wavelength of 1100nm, with a light source 2mm from the artery center. The artery is shown running underneath the surface in this example, though the artery depiction will be removed for the rest of the simulations to conserve space. The red dot on the surface represents the position of the light source. Each square represents a simulated detector (1mm x 1mm). The brighter colors represent a higher SNR, while the darker colors represent a lower SNR.

for blood tend to have lower a SNR since fewer photons make it to the detectors.

The next figure shows how the SNR changes as the light position changes. Because the 1100nm wavelength had the highest SNR of all the wavelengths, Fig. 3.3 uses this wavelength to demonstrate how the SNR shape changes with light source position. The maximum SNR of each wavelength is shown in Fig. 3.4.

The highest point for the SNR among all simulations is found at 1100nm when the light source and detector are both placed directly over the center of the artery. The detector would need to be placed 4mm away from the light source (as shown in Fig. 3.3). However, the spectrometer we are

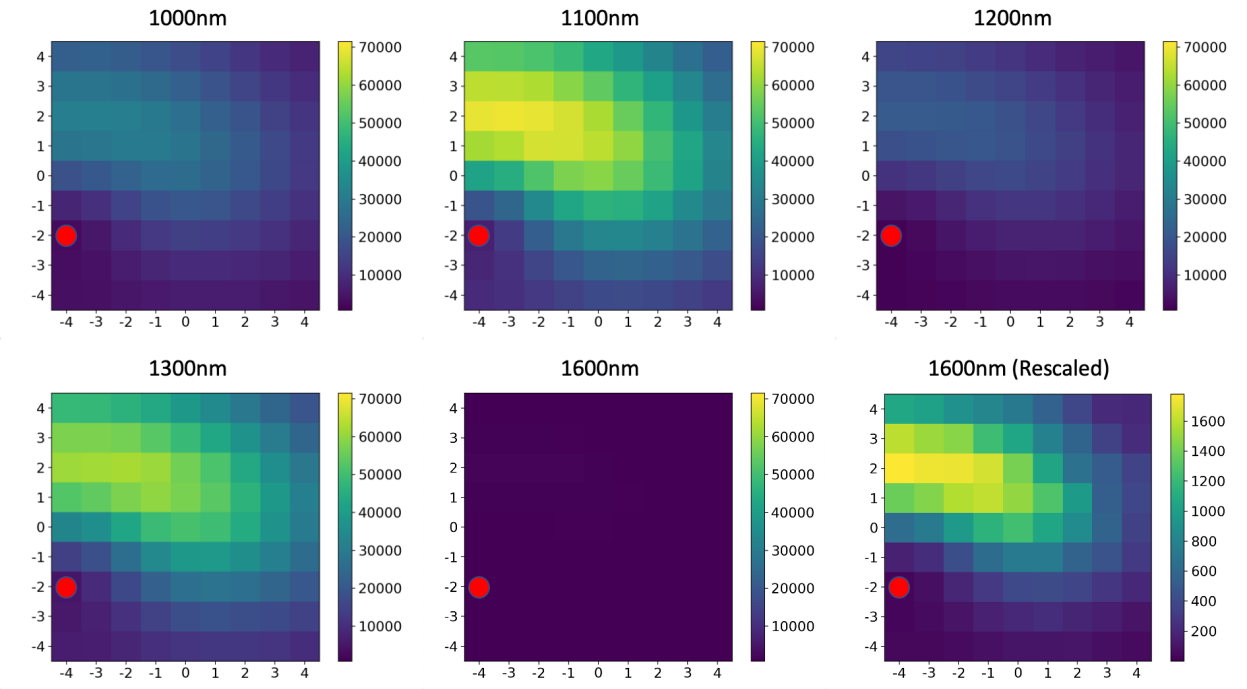


Figure 3.2 Each of these plots represents a simulation done with a different wavelength of light. The wavelengths for 1400nm and 1500nm were omitted because they are in the extinction coefficient for water and didn't have enough photons for analysis.

using for this project is not 1mm square. Instead, it is approximately 7mm long and relatively thin. This means that we want to find a line across the surface of the skin that is approximately 7mm long which has a high overall SNR. While our simulations only added detectors to the right of the light sources, remember that the geometry is symmetrical across the vertical line containing the light sources. This means that the results of the simulations are able to be mirrored to the left side. With this in mind, we determined that the ideal position for our light source is 2mm away from the artery, with the spectrometer directly across the artery 4mm away. (see Fig. 3.5) This result will be extremely helpful in the creation of the glucose sensor. These positions for the light source and spectrometer will ensure that as much signal as possible is coming from the light reaching the artery relative to the amount of shot noise we will be receiving.

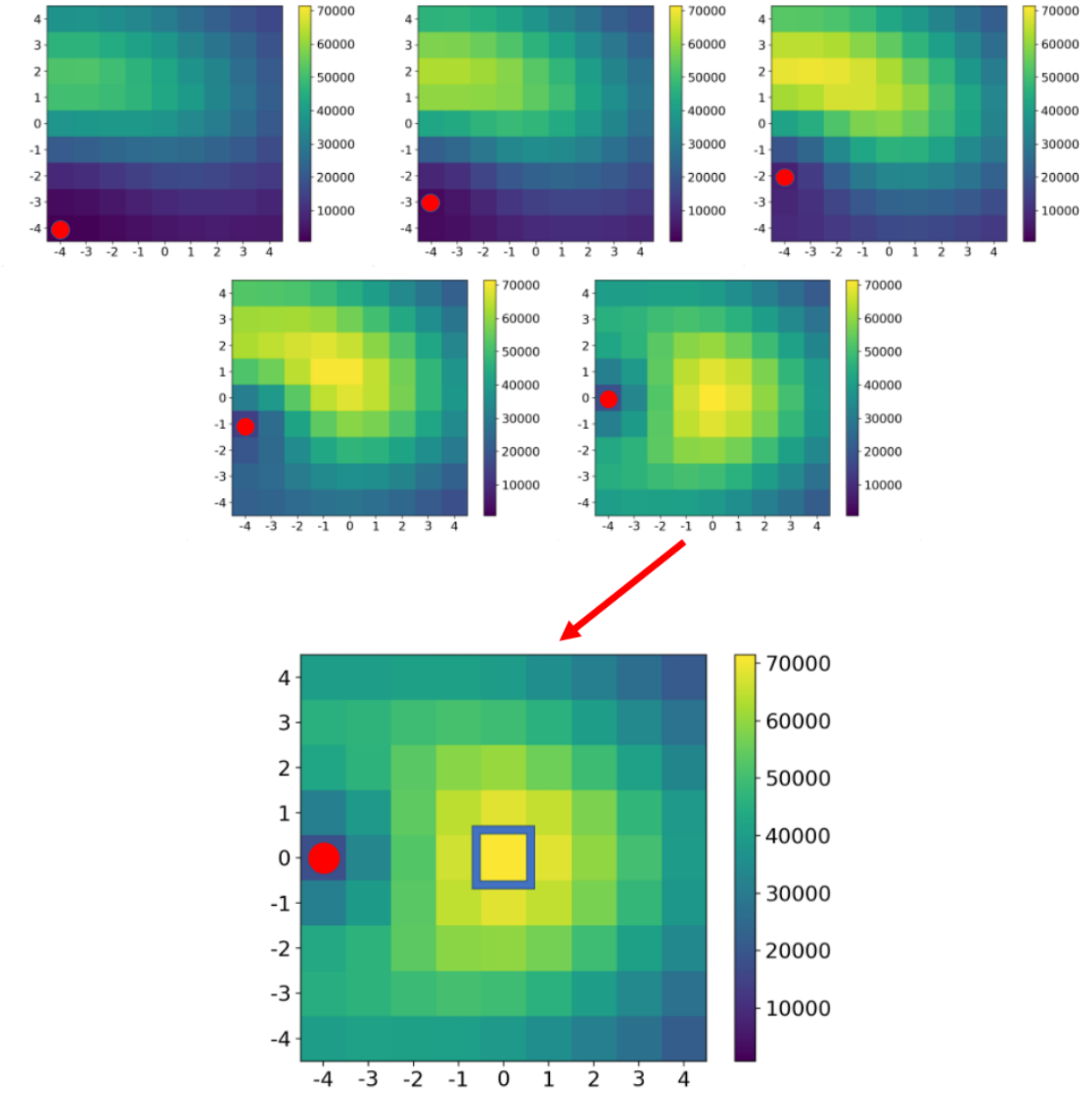


Figure 3.3 Each of these plots represent a simulation done with 1100nm light. The position of the light source was moved across the surface to show how SNR varies with light position. Since the SNR is maximized when the light source is directly over the artery, this plot is enlarged to show greater detail. The blue box represents the peak value of the SNR.

Wavelength (nm)	Maximum SNR
1000	32301.0
1100	71485.8
1200	21648.9
1300	63496.6
1600	1809.7

Figure 3.4 This table shows the maximum SNR for each wavelength. The peak value was always found when the light source was between 1mm and 2mm away from the artery.

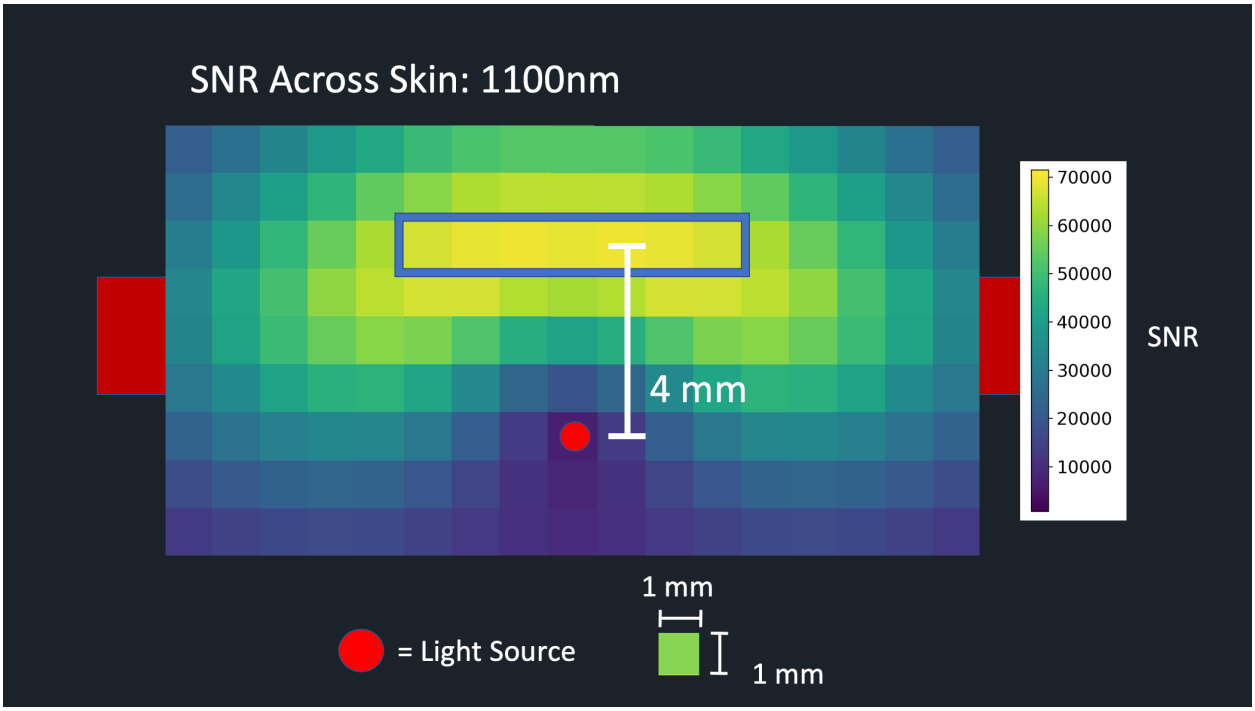


Figure 3.5 This is the simulation for 1100nm, with the light source positioned 2mm from the center of the artery. The gray box represents the ideal position for the spectrometer to maximize it's total SNR.

.1 Appendix

These graphs depict the simulations done for this project. The simulations for 1400nm and 1500nm were not included, since too few photons reached the detectors in the simulations. Most of those detectors received no signal, so an SNR could not be calculated. For an explanation of what each element of the figures represent, see Fig. 3.1.

The chart at the end of the Appendix shows the particular tissue parameters used in the Monte Carlo simulations. These values were taken from Bashkatov's paper on various biological optical properties [4].

The variable definitions are as follows:

μ_a = absorption coefficient

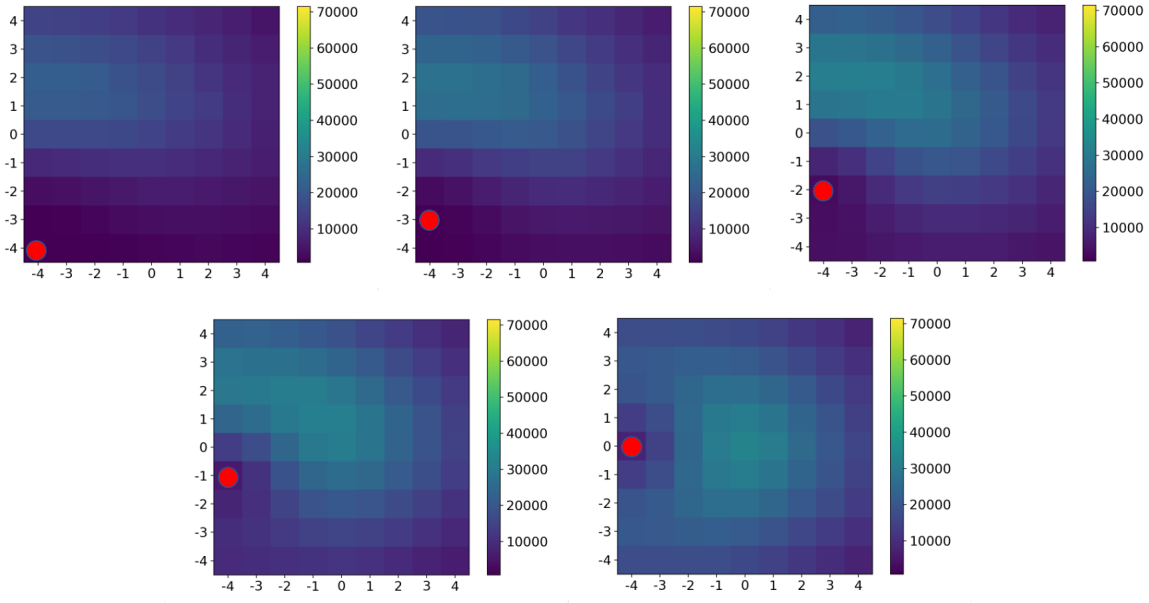
μ_s' = reduced scattering coefficient

μ_s = scattering coefficient

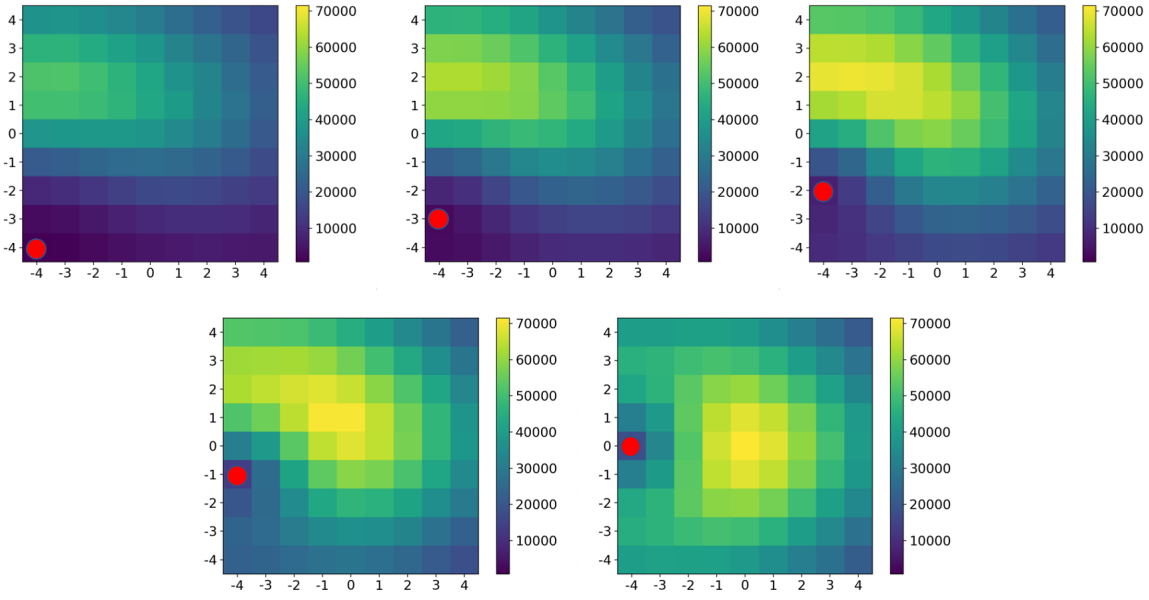
n = index of refraction

g = anisotropy factor

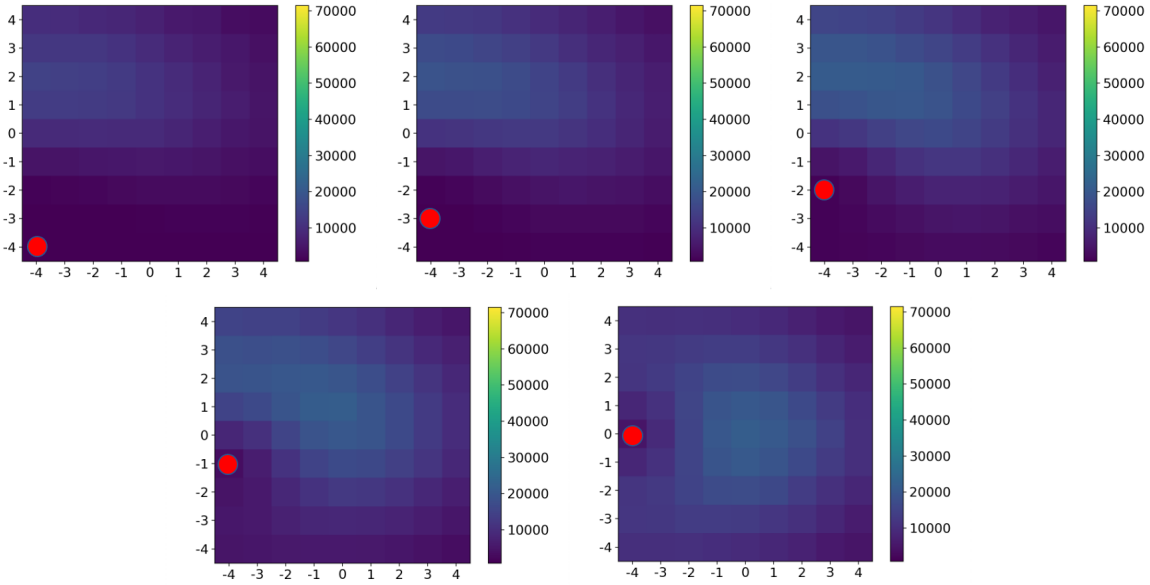
SNR: 1000 nm



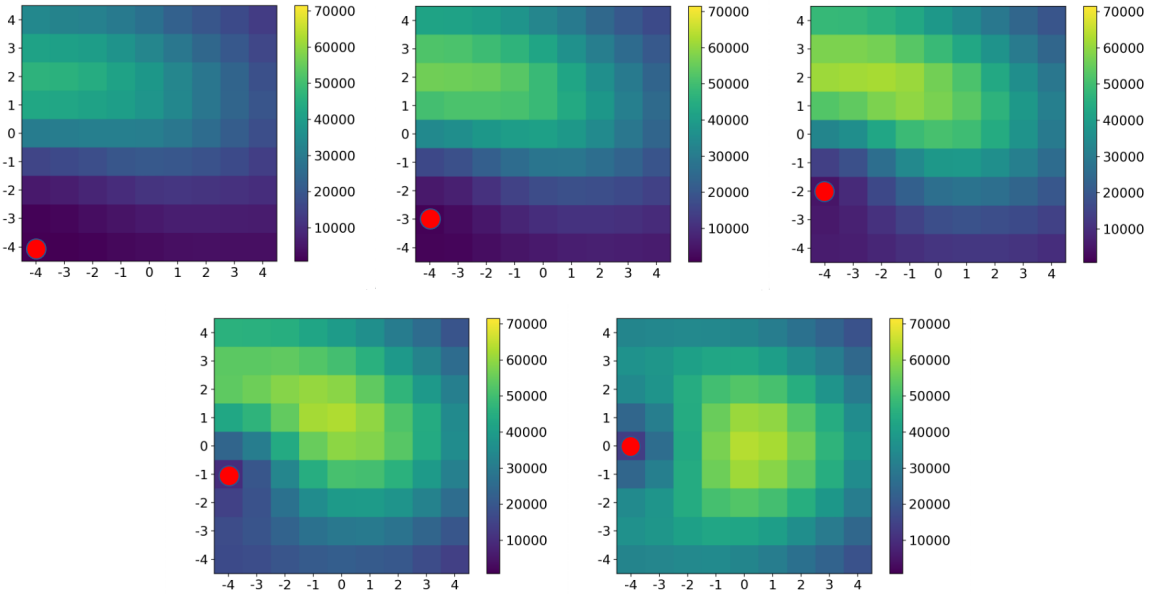
SNR: 1100 nm



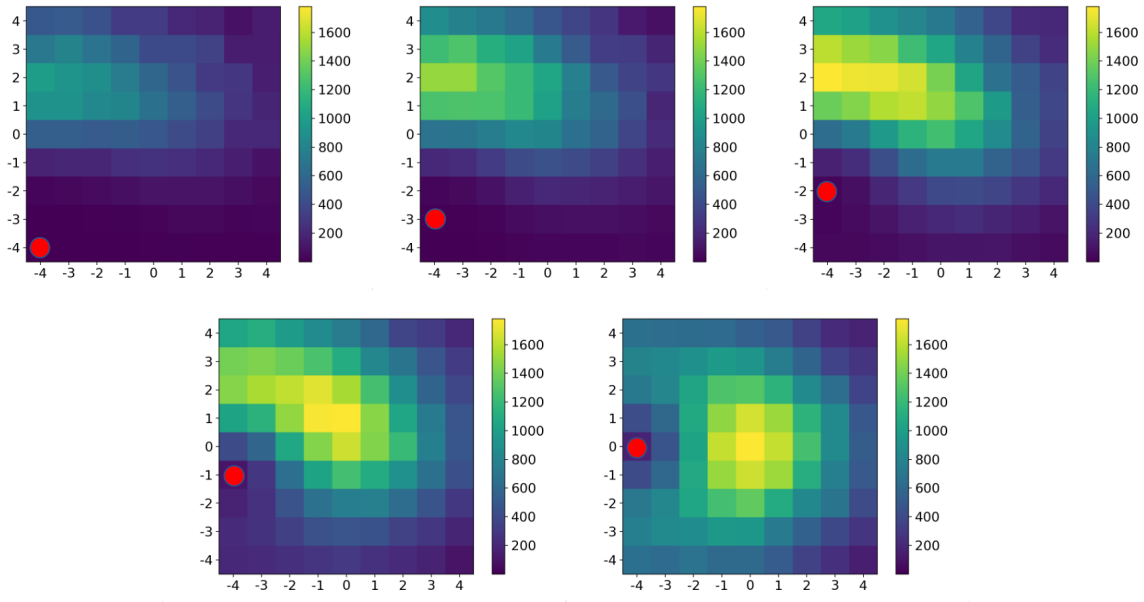
SNR: 1200 nm



SNR: 1300 nm



SNR: 1600 nm (Rescaled)



Wavelength	Skin μ_a	Skin μ_s'	Skin μ_s	Skin n	Skin g	Fat mu_a	Fat μ_s'	Fat μ_s	Fat n	Fat g	Blood μ_a	Blood μ_s'	Blood μ_s	Blood n	Blood g
1000	0.079	1.86	9.3	1.4	0.8	0.089	1.74	8.7	1.4	0.8	0.64	1.23042	61.83	1.4	0.9801
1100	0.046	1.76	8.8	1.4	0.8	0.074	1.66	8.3	1.4	0.8	0.35	1.17354	57.81	1.4	0.9797
1200	0.133	1.66	8.3	1.4	0.8	0.165	1.61	8.05	1.4	0.8	0.36	0.96048	55.2	1.4	0.9826
1300	0.119	1.62	8.1	1.4	0.8	0.105	1.58	7.9	1.4	0.8	0.19	1.00246	45.36	1.4	0.9779
1400	1.17	1.86	9.3	1.4	0.8	0.627	1.68	8.4	1.4	0.8	1.62	1.07828	39.21	1.4	0.9725
1500	1.75	1.99	9.95	1.4	0.8	0.852	1.76	8.8	1.4	0.8	1.71	1.12725	35.56	1.4	0.9683
1600	0.663	1.59	7.95	1.4	0.8	0.36	1.57	7.85	1.4	0.8	0.69	1.03611	32.48	1.4	0.9681

Bibliography

[1] T. Mathew, M. Zubair, and P. Tadi, "Blood Glucose Monitoring," StatPearls (2023).

[2] J. Harkness, "In Vitro Observation of Optical Changes in Whole Blood due to Injection of Glucose Solution," (2023).

[3] J. Cassidy, L. Lilge, and V. Betz, "FullMonte: a framework for high-performance Monte Carlo simulation of light through turbid media with complex geometry," Biomedical Applications of Light Scattering VII 8592 (2013).

[4] A. N. Bashkatov, E. A. Genina, V. I. Kochubey, and V. V. Tuchin, "Optical properties of human skin, subcutaneous and mucous tissues in the wavelength range from 400 to 2000nm," Journal of Physics D: Applied Physics **38,** 2543 (2005).

[5] B. Nedelec, N. J. Forget, T. Hurtubise, S. Cimino, F. de Muszka, A. Legault, W. L. Liu, A. de Oliveira, V. Calva, and J. A. Correa, "Skin characteristics: normative data for elasticity, erythema, melanin, and thickness at 16 different anatomical locations," SKIN RESEARCH AND TECHNOLOGY **22,** 263–275 (2016).

[6] K. K. Alsing and J. Serup, "High-frequency ultrasound skin thickness: Comparison of manual reading and automatic border detection includes assessment of interobserver variation of measurement," SKIN RESEARCH AND TECHNOLOGY **26,** 832–838 (2020).

[7] J. U. Kim, Y. J. Lee, J. Lee, and J. Y. Kim, "Differences in the Properties of the Radial Artery between Cun, Guan, Chi, and Nearby Segments Using Ultrasonographic Imaging: A Pilot Study on Arterial Depth, Diameter, and Blood Flow," EVIDENCE-BASED COMPLEMENTARY AND ALTERNATIVE MEDICINE 2015 (2015).

[8] S. Saito, H. Ikei, G. Hosokawa, and S. Tanaka, "Influence of the ratio between radial artery inner diameter and sheath outer diameter on radial artery flow after transradial coronary intervention," Catheterization and Cardiovascular Interventions **46,** 173–178 (1999).

[9] Z. Domagala, J. Grzelak, N. Pospiech, N. Hunter, J. Klekowski, A. Lach, K. Stoj, B. Kurc-Darak, and M. Trzaska, "Ultrasound evaluation of the radial artery in young adults - A pilot study," ANNALS OF ANATOMY-ANATOMISCHER ANZEIGER 238 (2021).

[10] V. MOOSER *et al.*, "NON-INVASIVE MEASUREMENT OF INTERNAL DIAMETER OF PERIPHERAL ARTERIES DURING THE CARDIAC CYCLE," JOURNAL OF HYPERTENSION **6,** S179–S181 (1988).